Local sympathetic denervation attenuates myocardial inflammation and improves cardiac function after myocardial infarction in mice

Karin A. Ziegler[1], **Andrea Ahles**[1,2], **Timo Wille**[3], **Julia Kerler**[1], **Deepak Ramanujam**[1,2], and **Stefan Engelhardt**[1,2]*

[1]Institute of Pharmacology and Toxicology, Technische Universität München, Biedersteiner Str. 29, Munich 80802, Germany; [2]DZHK (German Center for Cardiovascular Research), Partner Site Munich Heart Alliance, Biedersteiner Str. 29, Munich 80802, Germany; and [3]Bundeswehr Institute of Pharmacology and Toxicology, Neuherbergstr. 11, Munich 80937, Germany

Aims	Cardiac inflammation has been suggested to be regulated by the sympathetic nervous system (SNS). However, due to the lack of methodology to surgically eliminate the myocardial SNS in mice, neuronal control of cardiac inflammation remains ill-defined. Here, we report a procedure for local cardiac sympathetic denervation in mice and tested its effect in a mouse model of heart failure post-myocardial infarction.
Methods and results	Upon preparation of the carotid bifurcation, the right and the left superior cervical ganglia were localized and their pre- and postganglionic branches dissected before removal of the ganglion. Ganglionectomy led to an almost entire loss of myocardial sympathetic innervation in the left ventricular anterior wall. When applied at the time of myocardial infarction (MI), cardiac sympathetic denervation did not affect acute myocardial damage and infarct size. In contrast, cardiac sympathetic denervation significantly attenuated chronic consequences of MI, including myocardial inflammation, myocyte hypertrophy, and overall cardiac dysfunction.
Conclusion	These data suggest a critical role for local sympathetic control of cardiac inflammation. Our model of myocardial sympathetic denervation in mice should prove useful to further dissect the molecular mechanisms underlying cardiac neural control.
Keywords	Neuroimmune system • Myocardial infarction • Sympathetic nervous system

1. Introduction

Cardiac function is under tight control of the autonomic nervous system (ANS) with its parasympathetic and sympathetic branches.[1,2] The sympathetic control of myocardial contractile force, frequency, and conduction has been analysed in great detail, as has been the regulation of vascular tone.[3] Comparably, little is known about the sympathetic control of cardiac non-myocytes including immune cells, which are subject to sympathetic control in other organs.[4,5] In agreement with its central role in cardiac physiology, targeting effector pathways of the sympathetic nervous system (SNS) has evolved as a cornerstone of medical therapy for a number of cardiac conditions. Chronic heart failure is accompanied by activation of the SNS, which by itself is a strong negative predictor of

outcome.[6,7] Antagonists at beta1-adrenoceptors—one of the main receptors for norepinephrine released by sympathetic nerve endings—prevent these detrimental effects and effectively reduce mortality in heart failure. Beta1-adrenoceptor antagonists are similar standard therapy to prevent heart failure after myocardial infarction (MI). The latter has been shown to exert drastic changes of the cardiac SNS, with a transient loss of myocardial sympathetic innervation followed by a phase of overshooting nerve remodelling (also termed hyperinnervation[8–10]).

MI also triggers a massive inflammatory response characterized by early neutrophil invasion followed by monocyte/macrophage recruitment.[11–13] Mutual control of MI-induced sympathetic remodelling and the cardiac inflammatory response has been proposed. It is unclear, at present, whether cardiac immune cells regulate sympathetic

* Corresponding author. Tel: +49 89 41403260; fax: +49 89 41403261, E-mail: stefan.engelhardt@tum.de

reinnervation[14] or whether the SNS controls immune cell accumulation.[15]

The mammalian myocardium receives terminal sympathetic nerve fibres from several ganglionic structures, namely the superior cervical ganglia (SCGs), the stellate ganglia, and upper thoracic ganglia (until Th6[16,17]). Their efferent branches to the heart (extrinsic sympathetic nervous system) project to all vessels and regions of the myocardium where they form an intricate network with each other (intrinsic sympathetic nervous system[18]) and also with vagal nerve endings.[19] Therefore, in the adult heart, single sympathetic nerve fibres cannot be traced to a defined extracardiac ganglionic structure.[20] However, it is well established that in mice within the ventricular myocardium, the stellate ganglion primarily projects to the dorsal side, whereas the SCG preferentially innervates the anterior myocardium.[20] This part of the ventricle is nourished by the left anterior descending artery (LAD), whose obstruction is the most frequent basis of large transmural infarctions.[21]

A current obstacle towards the elucidation of the mechanisms underlying these intriguing observations and questions is the lack of methodology to specifically and locally interfere with the myocardial SNS. We therefore aimed to establish an animal model in mice that would allow primarily for denervation of the anterior ventricular wall. Upon validating its effectiveness in reducing myocardial sympathetic nerve density, we tested its effect in a mouse model of heart failure post-myocardial infarction.

2. Methods

2.1 Animal models

All mice used were on a C57BL6/N genetic background. MI was induced on 8–10-week-old male mice. Subcutaneous injection of buprenorphine (0.08 mg/kg) was used for preoperative and postoperative analgesia. Mice were anaesthetized in an induction chamber with 4% isoflurane mixed with 0.5 L/min of 100% O_2, while the anaesthesia during the surgery was maintained at 1.5% isoflurane with 0.5 L/min O_2. To maintain the body temperature, the mice were operated on a heating plate (36 °C). Partial thoracotomy was performed, and the pericardium was opened. MI was induced by ligation of the proximal part of the LAD using an 8.0 silk suture. In sham surgery, only the chest and pericardium was opened but no LAD ligation was carried out.

The technique of the SCG removal (SCGx) was performed as described previously for rats.[22] After induction of anaesthesia and intubation, a vertical neck incision (~10 mm) was made and kept open using placeholders. Next, the salivary glands were carefully dissected from the caudal adhesive tissue and flipped aside. The position was then corrected by adjusting the lower two placeholders (with expanded surface). With blunt forceps, the sternocleidomastoid muscle was lifted, moved aside, and held using the upper two, thinner placeholders. Lateral positioning of the sternocleidomastoid muscle allowed for clear visibility of the carotid artery. The common carotid artery (CCA) was followed in cranial direction to locate the carotid bifurcation (in internal and external carotid arteries). The almond-shaped SCG is located behind the carotid bifurcation. This approach exposed the preganglionic and postganglionic branches of the SCG, facilitating complete removal of the ganglion itself. The ganglionic cell body was fully extracted by shifting the external carotid artery to the lateral side using a special 90° angled forceps. Finally, the SCG was detached from the sympathetic chain and the SCG tissue was collected (*Figure 1A*). Complete cardiac sympathetic denervation was achieved by additional removal of the SCG on the contralateral side. The SCG should never be extracted from the ventral side, as this may damage the carotid artery resulting in bleeding and cerebral infarction in mice.[22] In a combined SCGx and MI surgery (MI + SCGx), bilateral ganglionectomy (SCGx) was performed first followed by LAD ligation (MI). Fourteen days after the intervention, mice were euthanized by cervical dislocation after echocardiographic measurement and under anaesthesia with isoflurane. The survival rates for MI alone and MI + SCGx were comparable as well as for sham and SCGx alone. After SCGx removal, no behavioural abnormalities could be observed.

Blood samples were obtained from retrobulbar venous plexus 24 h after surgery. Mice were therefore anaesthetized with isoflurane. For plasma extraction, blood was collected in heparinized tubes and centrifuged at 2000 ×g for 5 min. Troponin T was determined by a high-sensitive cardiac troponin t (hs-cTnT) assay based on chemiluminescence. These measurements were performed at the German Heart Centre Munich.

All animal studies were performed in accordance with relevant guidelines from the Directive 2010/63/EU of the European Parliament on the protection of animals used for scientific purposes. Approval for all animal experiments was granted by local authorities (Regierung von Oberbayern).

2.2 Echocardiography

Cardiac function was assessed by transthoracic echocardiography. Echocardiographic monitoring was carried out before surgery and at the end of the experiment before the tissue was harvested. Ultrasound gel was applied to the clean-shaved chest of isoflurane-anaesthetized mice. For preoperative preparation, the shaving included not only the chest but also the neck, dependent on the surgical intervention (for SCGx and MI + SCGx). Echocardiography was carried out using an ultrasound system with a linear transducer with 32–55 MHz frequency (VisualSonics, Toronto, Canada) combined with Vevo 770 software. B-mode tracings in the long-axis views were recorded, and dimensions of systolic and diastolic myocardium were measured. Parameters are calculated according to the VisualSonics standard measurements and calculations. Echocardiographic speckle-tracking-based strain imaging was analysed with the Vevo strain software as previously described.[23,24] Two cardiac cycles, which were not disturbed by respiration or other interruptions, were selected. Next, in the long-axis B-mode picture, endocardial and epicardial traces were delineated and reviewed. In case of deviations, the trace was adjusted accurately to the wall movement.

2.3 Histochemical and immunohistochemical analyses

Cryosections (10 μm) of LV myocardium were stained with Sirius Red/Fast Green as previously described.[25] Whole heart images were taken with a 10× objective using an AxioObserver Z1 (Zeiss, Oberkochen, Germany) motorized scanning stage microscope (130 × 85; Märzhäuser). MetaMorph software (version 7.7; Molecular Devices, Sunnyvale, CA, USA)) was applied for scar quantification. Infarct scar was measured as the ratio of Sirius Red to Fast Green signals in each section.

For the analysis of immune cells and nerve formation, myocardial sections (20 μm) were fixed with acetone for 15 min at -20 °C (CD68, actinin, tyrosine hydroxylase (TH)] or 5% paraformaldehyde (PFA) for 10 min at room temperature [CD45, CD3, and Ly6G]. After permeabilization with 1% Triton-X and blocking with 5% bovine serum albumin, sections were incubated with primary antibodies against CD68 (AbD Serotec, Raleigh, NC, USA; catalogue number: MCA1957), CD45
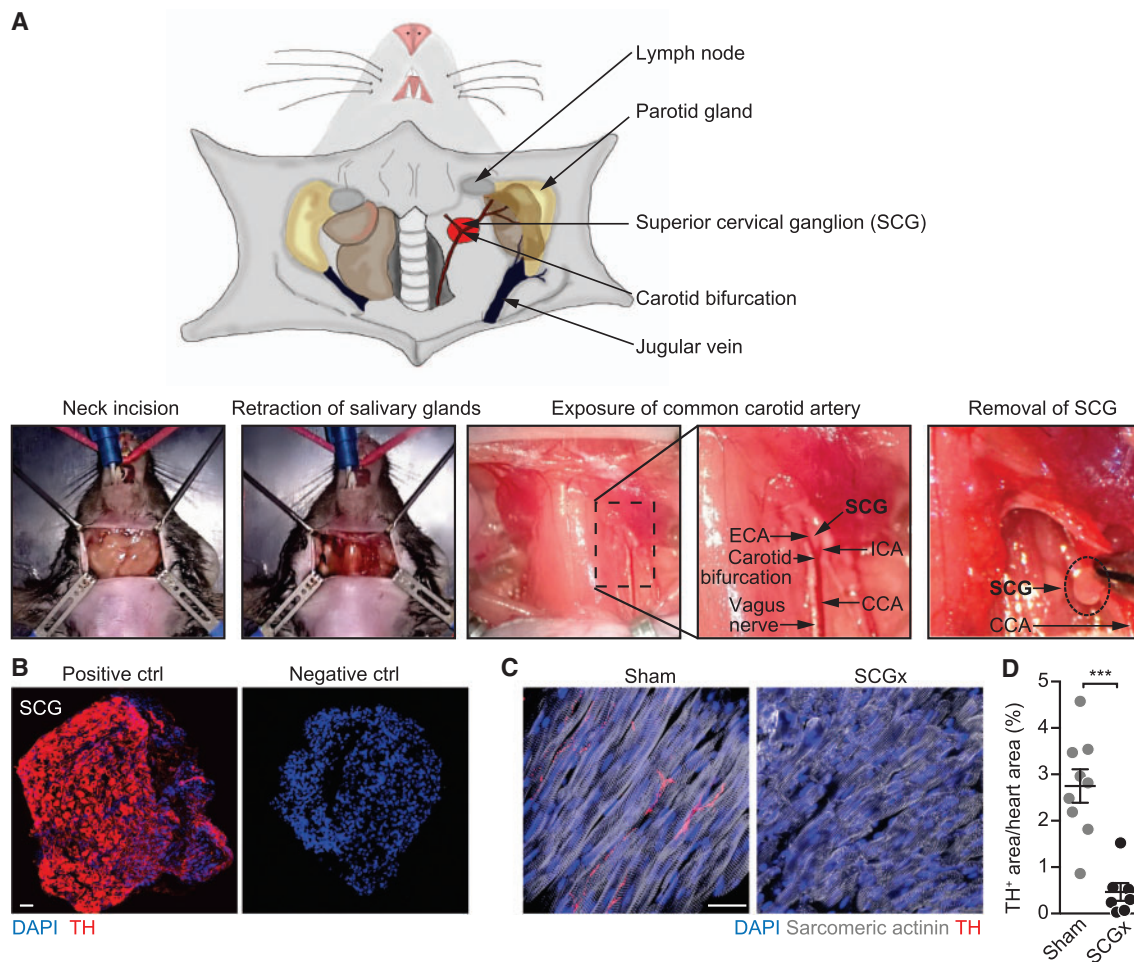
Figure 1 Surgical removal of the SCGs in mice. (*A*) (Upper panel) Scheme depicting the anatomical location of the SCG (red) and neighbouring structures. For better overview, the sternocleidomastoid muscle has not been pictured. (Lower panels) Surgical procedure of SCG removal (SCGx). A vertical incision is applied to the skin of the clean-shaved neck at the height of the cervical vertebrae C1/C2. Exposed glandular tissue and the sternocleidomastoid muscle are then pulled to the side to expose the CCA. The SCG is located behind the bifurcation of the CCA into the internal (ICA) and the external carotid artery (ECA). Next to the CCA, the vagal nerve is situated. Finally, the preganglionic and postganglionic nerves of the SCG are cut with a scissor and the ganglion is removed. (*B*) Immunofluorescent staining of surgically removed SCG. The same staining procedure served as a negative control, except that the primary antibody was omitted. Tyrosine hydroxylase (TH), scale bar: 50 μm. (*C*) Heart sections stained for sympathetic nerves (TH) in mice with ganglionectomy (SCGx) and control mice (sham), scale bar: 20 μm. (*D*) Quantification of TH-positive area. Data are mean ± SEM of $n = 9$ (sham) and $n = 7$ mice (SCGx). Student's *t*-test was applied for statistical analysis. ****P* < 0.001.

(Abcam, Cambridge, UK; catalogue number: AB23910), CD3 (Abcam, catalogue number: ab16669), Ly6G (BD Pharmingen, Franklin Lakes, NJ, USA; catalogue number: 551459), sarcomeric actinin (Abcam, catalogue number: ab68167) or TH (Millipore, Burlington, MA, USA; catalogue number: AB152) overnight at 4 °C. Nuclei were detected by staining with 4′, 6-diamidino-2-phenyldole (DAPI). The sections were then incubated with respective secondary antibodies conjugated to either Alexa Fluor 488 (goat anti-rabbit immunoglobulin G (IgG); Life Technologies, Carlsbad, CA, USA; catalogue number: A-11034) or 594 (donkey anti-rat IgG, Life Technologies catalogue number: A-21209).

For immune cell count whole heart images were obtained as described earlier for the Sirius Red/Fast Green staining. TH images were taken with the 63× objective. CD45, CD68, Ly6G, and CD3-positive cells were measured after defining the width (4–35 μm) of the marked cells. These data were normalized to the number of nuclei, which was acquired by counting the DAPI-positive dots. The quantification of nerve density was obtained using the angiogenesis tube formation tool of the MetaMorph software.

Cardiac myocyte hypertrophy was assessed by staining 10 μm slices of LV myocardium with Alexa Fluor 647-conjugated wheat germ agglutinin (WGA). Sections were washed with phosphate-buffered saline, fixed with 5% PFA for 10 min at room temperature, and incubated with WGA for 1 h. Sytox green (incubation at room temperature for 10 min) was used to detect nuclei. Images were acquired using confocal microscopy (Leica TCS SP5 II) and then analysed with the MetaMorph software.[26] For each heart, an average of three images from different regions of the LV, in the setting of LAD ligation only images from the remote area were taken.

2.4 Quantitative real-time polymerase chain reaction

RNA was prepared from the tissue samples using the peqGOLD RNApure (peqlab, Erlangen, Germany), then 500 ng of RNA was reverse

transcribed with Protoscript reverse transcriptase (NEB, Frankfurt am Main, Germany), as defined by the manufacturers' manuals. Application of FastStart universal SYBR Green master mix (Roche, Basel, Switzerland) was used to amplify target complementary DNA sequences by quantitative real-time polymerase chain reaction (PCR). The target messenger RNA (mRNA) was flanked by the specific primers listed below to examine gene expression in the tissue. For the validation of primer specificity, the dissociation curve was plotted. A single well contained a total volume of 12.5 μl consisting of 1× SYBR Green master mix, 10 pmol of each primer, and 10 ng of template. With the StepOnePlus Real-Time PCR system (Applied Biosystems, Waltham, MA, USA) PCR was executed.

The following primer sequences for murine tissue were used (gene subsequent sequences of forward and reverse primers): *Cx3cr1* (5′-TGC CTT CTT CCT CTT CTG GA-3′, 5′-TAA AGG GGT TGA GGC AAC AG-3′); *HPRT* (5′-GCA GTA CAG CCC CAA AAT GG-3′, 5′-AAC AAA GTC TGG CCT GTA TCC AA-3′), *Tnf-α* (5′-CGA GTG ACA AGC CTG TAG CC-3′, 5′-GGT GAG GAG CAC GTA GTC G-3′), and *Il-10* (5′-AGC TGA AGA CCC TCA GGA TG-3′; 5′-TGG CCT TGT AGA CAC CTT GG-3′).

2.5 Western blotting

Tissue lysates were acquired by direct lysis at 4 °C in a 50 mM Tris buffer (pH 6.7) comprising 2% SDS, 1 mM Na_3VO_4 and protease inhibitor (Thermo Fisher, Waltham, MA, USA). Corresponding to protein size, the proteins (10–20 μg) were separated by SDS-polyacrylamide gel electrophoresis in gels containing 10–12% acrylamide, followed by western blotting as described previously.[27] Primary antibodies against nerve growth factor (NGF; catalogue number: sc-548) and Hsp90 (catalogue number: sc-13119) were obtained from Santa Cruz (Dallas, TX, USA), secondary antibodies raised against rabbit (catalogue number: 111-035-144) and mouse (catalogue number: 115-035-003) from Dianova (Hamburg, Germany). The bands were quantified using Multi Gauge software. Hereby the AU (arbitrary unit)-BG (background) values of pro-NGF were divided through values of HSP90 after background subtraction.

2.6 Statistical analysis

Data was presented as mean ± SEM. Statistical analysis was performed using GraphPad Prism software package (version 6). Data distribution was assessed by D'Agostino-Pearson omnibus test, Shapiro–Wilk test, and Kolmogorov–Smirnov test for normality. Differences between the two means were tested using two-tailed unpaired Student's *t*-test for Gaussian distributed data. Analysis of variance followed by Bonferroni test (normal distributed data set) or Kruskal–Wallis test (non-normal distributed data set) were used as appropriate and indicated in the figure legend. $P < 0.05$ was considered statistically significant.

3. Results

3.1 Surgical removal of the SCGs effectively reduces sympathetic innervation of the LV myocardium

Mice were anaesthetized and intubated before neck incision and retraction of the salivary glands (*Figure 1*). Next, the sternocleidomastoid muscle was drawn back with a placeholder to expose the common carotid artery (CCA). Following the CCA in cranial direction, the carotid bifurcation was localized and bluntly prepared from its underlying tissue.

The external carotid artery (ECA) was then carefully flipped laterally to expose the SCG, which can then be localized directly underneath the carotid bifurcation (lower panel in *Figure 1A*). Next, the upper (preganglionic) and the lower (postganglionic) branches were cut with a scissor and the now disconnected ganglion removed. The same procedure was then repeated on the contralateral side (see also Methods for further details on surgical methodology). To validate that the removed structure indeed contained the ganglionic sympathetic neurons, we stained cryosections with an antibody directed against TH (*Figure 1B* left panel), the rate-limiting enzyme during catecholamine synthesis and a specific marker for the SNS.[28] All of the putative ganglionic structures tested with this procedure ($n = 7$) stained positive for TH with no signal detectable in the absence of the primary antibody (right panel in *Figure 1B*). We then used staining for TH to detect and quantify the presence of sympathetic nerve endings in the lower anterior wall of the left ventricle and to determine the effect of bilateral surgical removal of the SCG (*Figure 1C*). Fourteen days after bilateral SCGx, we found the lower LV wall to be essentially devoid of any immunoreactivity for nerve endings compared to the base region of the anterior wall or sham-operated animals. Unilateral SCGx indicated that the left and right SCGs comparably contribute to the sympathetic innervation of the anterior wall (see Supplementary material online, *Figure S1*).

3.2 Sympathetic denervation prevents cardiac myocyte hypertrophy after MI

We next sought to determine the effect of sympathetic denervation of the anterior wall on the development of myocardial remodelling and inflammation in this region and examine to what extent it affects global cardiac function following MI. *Figure 2A* provides a scheme depicting the experimental outline. Three days prior to MI surgery, echocardiography was taken, and the animals were randomly assigned to one of the four different groups, i.e. a sham group, a sympathetic denervation group (SCGx), an MI group (MI) and an MI group with concomitant sympathetic denervation (MI + SCGx). Twenty-four hours post-surgery, troponin T levels were determined in venous blood samples, and the animals were then followed up for a total of 2 weeks before functional analysis by echocardiography and harvesting of the tissue (*Figure 2A*). Determination of plasma troponin T (cTnT) determined 24 h after LAD ligation were similar between mice subjected to MI alone compared to those with concomitant sympathetic denervation, indicating that the ischaemic loss of cardiac myocytes was similar in both groups (*Figure 2B*). In a first series of analyses, we then sought to assess the effect of sympathetic denervation on scar formation and structural remodelling (*Figure 2C–E*). Planimetric determination of infarct sizes in tissue sections stained with Sirius Red/Fast Green indicated medium- to large-sized infarcts in both MI groups. MI induced significant cardiac hypertrophy (as evidenced by an increase in heart weight-to-tibia length ratio) in control treated mice but not in mice subjected to sympathectomy (*Figure 2E*), albeit the inherent variation of this parameter did not allow for statistical significance upon comparison of the MI and MI + SCG groups. However, quantitative analysis of cardiac myocyte dimensions in sections stained with the membrane stain WGA revealed a prominent and highly significant inhibition of MI-induced cardiac myocyte growth upon denervation (*Figure 2F*). To assess whether removal of the SCGs had led to effective sympathetic denervation of the LAD region also after MI, we stained tissue sections from this region for TH as in *Figure 1* and determined the protein levels of nerve growth factor precursor (pro-NGF) by western blotting of myocardial protein lysates. Consistent with our results
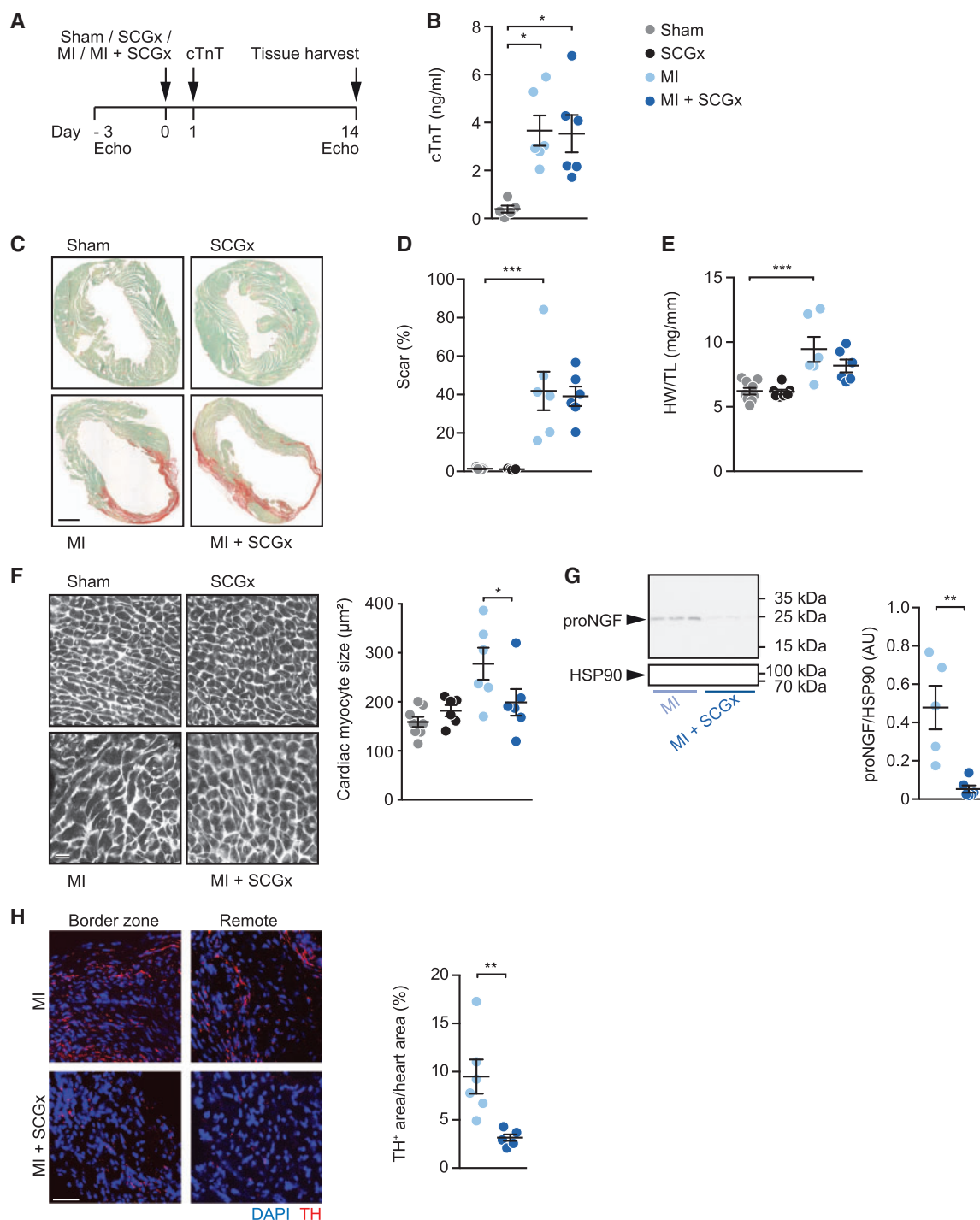
Figure 2 Sympathetic denervation attenuates cardiac hypertrophy after MI. (A) Experimental set-up. Intervention groups included sham, SCGx (bilateral removal of the SCG), MI (myocardial infarction by LAD ligation), and MI + SCGx (bilateral SCG-removal followed by LAD ligation). Three days prior to surgical intervention, cardiac function was assessed by echocardiography. Twenty-four hours after surgery, plasma troponin levels were measured. Functional analysis and tissue harvesting was performed 14 days after the intervention. (B) Cardiac troponin T (cTnT) values determined in plasma 24 h after surgery. (C) Myocardial paraffin sections stained with Fast Green/Sirius Red. Scale bar: 1 mm. (D) Quantification of Sirius Red-positive area. (E) Heart weight-to-tibia length ratio. (F) WGA staining for quantification of cardiac myocyte dimensions. Scale bar: 50 µm. (G) Representative immunoblot of pro-NGF expression in LV myocardium after MI and MI + SCGx and quantitative analysis of the data. (H) Quantification of intramyocardial nerves within the LV anterior wall by staining with an antibody directed against TH. Data are mean ± SEM of n = 9 (sham), n = 7 (SCGx) and n = 6 mice (MI, MI + SCGx). cTnT values were analysed with the Kruskal–Wallis-test. *P < 0.05 vs. respective sham. Two-way analysis of variance with Bonferroni's multiple comparison test was applied for statistical analysis of scar formation, heart weight-to-tibia length ratio and cardiac myocyte size. *P < 0.05, **P < 0.01, ***P < 0.001. Mann–Whitney test was used for analysis of pro-NGF/HSP90 and TH-positive area. ***P < 0.001 vs. MI.
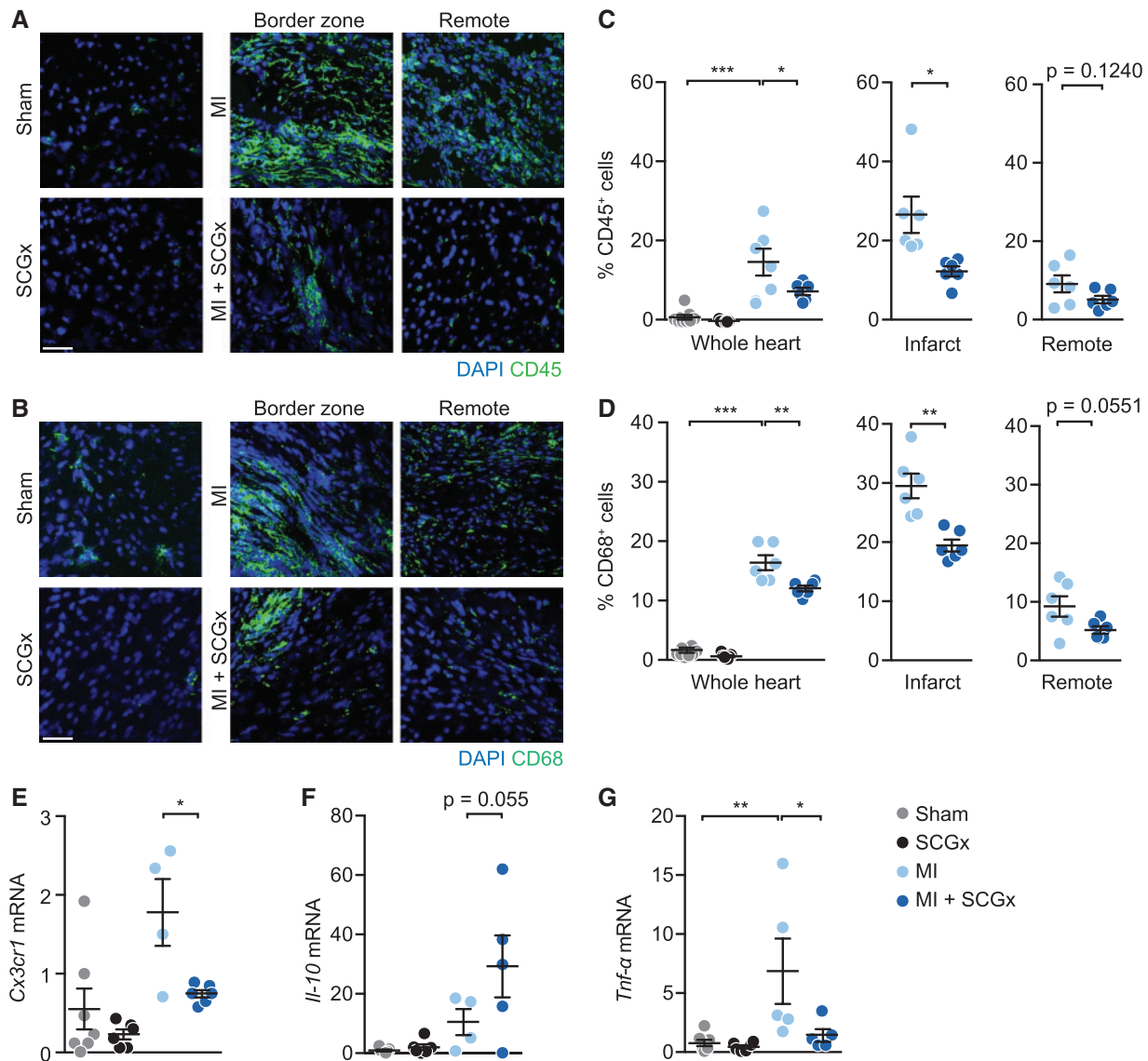
Figure 3 Reduced inflammatory cell infiltration upon sympathetic denervation. (*A*, *B*) Representative confocal images of LV tissue sections 14 days after the respective intervention stained with DAPI and anti-CD45 antibody (*A*) or anti-CD68 antibody (*B*). (*C*) Quantification of CD45- and (*D*) CD68- cells (% of DAPI-positive cells) in whole heart, infarct and remote area. Scale bar: 50 μm. Data are mean ± SEM of $n = 9$ (sham), $n = 7$ (SCGx), and $n = 6$ mice (MI, MI + SCGx). (*E–G*) Determination of inflammation-related mRNAs by PCR in total RNA prepared from LV myocardium from the indicated groups. Relative expression of (*E*) CX3C chemokine receptor 1 (*Cx3cr1*), (*F*) interleukin-10 (*Il-10*) and (*G*) tumour necrosis factor alpha (*Tnf-α*). The mRNA levels were first normailzed to *Hprt* and then further normalized to the levels in sham. All four groups were compared by two-way analysis of variance with Bonferroni's multiple comparison test. *$P < 0.05$, **$P < 0.01$, ***$P < 0.001$. MI and MI + SCGx groups were analysed with Student's *t*-test. *$P < 0.05$ and **$P < 0.01$ vs. MI.

obtained in non-infarcted animals (*Figure 1*), local sympathetic denerva-tion (SCGx) resulted in a drastic reduction of pro-NGF levels (*Figure 2G*) and reduced staining for TH (*Figure 2H*).

3.3 Reduced inflammatory cell infiltration upon sympathetic denervation

Because MI triggers a massive inflammatory response, we sought to determine whether it is dependent on local sympathetic regulation. To this end, we examined the number of CD45 (common marker for leuco-cytes) and CD68 (macrophage marker)-positive cells in LV myocardium

of animals from the four different study groups. As expected, MI induced a prominent and long-lasting myocardial infiltration of inflammatory cells, the majority of which stained positive for CD68, identifying them as mac-rophages (*Figure 3*). SCG removal led to a significant decrease of these cells (*Figure 3A–D*). Interestingly, tendencies to reduced numbers of mac-rophages after SCG were also observed in non-infarcted animals and in the non-ischaemic (remote) myocardium of infarcted hearts (grey sym-bols in *Figure 3* left panel and blue symbols in *Figure 3* right panel). The mRNA levels of the macrophage marker *Cx3cr1* and the pro-inflammatory cytokine *Tnf-α* were reduced coinciding with an increase of
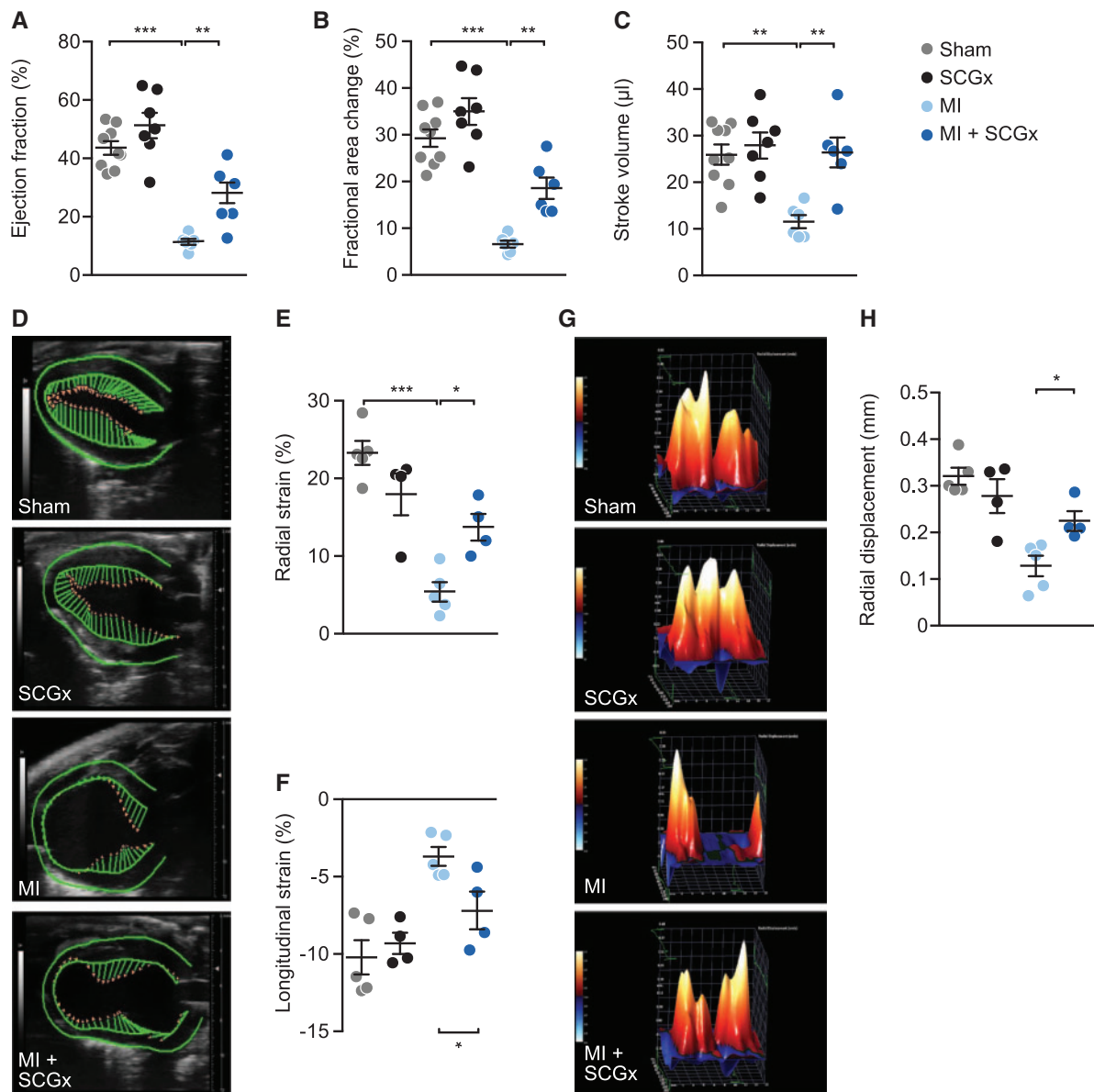
Figure 4 Local sympathetic denervation improves cardiac function after myocardial infarction. (A) Ejection fraction, (B) fractional area change, and (C) stroke volume determined by echocardiography. Data are mean ± SEM of $n = 9$ (sham), $n = 7$ (SCGx), and $n = 6$ mice (MI, MI + SCGx). All four groups were compared by two-way analysis of variance with Bonferroni's multiple comparison test. **$P < 0.01$, ***$P < 0.001$. (D–H) Analysis of myocardial strain by echocardiography-based speckle tracking. (D) Vector mapping of LV function. (E) Quantification of radial and (F) longitudinal strain by time-to-peak analysis. (G) 3D reconstruction of radial displacement in a single cardiac cycle. (H) Quantification of radial displacement in the time to peak analysis. Shown are mean ± SEM from $n = 5$ (sham, MI) and $n = 4$ (SCGx, MI + SCGx) mice. All four groups were compared by two-way analysis of variance with Bonferroni's multiple comparison test. *$P < 0.05$, ***$P < 0.001$.

the anti-inflammatory molecule *Il-10* upon sympathetic denervation and LAD ligation (*Figure 3E–G*). Other immune cells, e.g. neutrophils and T cells, were present at much lower numbers (<1.5% vs. up to 30% for macrophages, see Supplementary material online, *Figure S2*).

3.4 Local sympathetic denervation improves cardiac function after MI

Finally, we assessed the effect of sympathetic denervation of the anterior wall on global cardiac function and the functional impairment following MI. Fourteen days after the intervention echocardiography

revealed significantly improved cardiac function of mice subjected to combined MI and SCGx compared with MI alone (*Figure 4A–C*). Sympathectomy may be expected to affect cardiac frequency. To determine whether the later was indeed the case, we analysed among other parameters the heart rate of all four groups and found it to be essentially unchanged (see Supplementary material online, *Figure S3*). In addition, we determined LV strain as a sensitive measure for LV function, which is less operator dependent and independent from LV hypertrophy (*Figure 4D–H*). LV strain imaging indicated better LV global myocardial function, with significant higher radial (*Figure 4E*)

and longitudinal (*Figure 4F*) strain and radial displacement (*Figure 4G* and *H*) in mice subjected to MI and SCGx compared to MI alone.

4. Discussion

Chronic activation of the SNS occurs in heart failure and has been identified as a key pathophysiological element contributing to disease progression.[29] Consequently, the SNS has been the target of a wide variety of therapeutic interventions in a number of clinical conditions.[30] While current standard therapeutic regimens (such as beta-blockers) aim at the effector cellular pathways of the SNS, therapeutic strategies directly inhibiting SNS function have been less successful.[31] For example, experimental global sympathetic denervation using 6-hydroxydopamine (6-OHDA) had adverse effects on cardiac function and remodelling[32] and also pharmacological inhibitors of sympathetic tone exerted limited clinical efficacy.[6] As an alternative to systemic inhibition of the SNS, a number of approaches have been developed that aim at the local interference with the sympathetic innervation of the heart.[33] These include the surgical removal of the stellate ganglion (stellectomy[34,35]) or injection of ethanol into the latter (chemical sclerosis[36]).

Most recently, data from Manousiouthakis *et al.*[20] suggested that the LV anterior wall is innervated by sympathetic nerves derived from the SCG. However, whether selective interference with SCG-derived sympathetic innervation would affect the cardiac response in disease has not been tested till date, hindering mechanistic studies as to the molecules and cells involved in the cardiac response to sympathetic activation.

In this study, we have developed an approach to interfere with the sympathetic innervation of the LV anterior wall in the mouse. Our method permits a simple, fast, and selective intervention, allowing us to address the role of local sympathetic control in post-MI cardiac dysfunction. SCG removal effectively prevented cardiac dysfunction together with a reduction of cardiac macrophage numbers. These findings suggest that indeed neuroimmune crosstalk occurs in the heart and that it may determine cardiac remodelling and dysfunction. As our experiments do not provide formal proof of direct nerval control of myocardial immune cells, other myocardial cell types may also be involved, an interesting topic for future studies.

The immune and the nervous systems intensely interact and mutually control each other.[37] In peripheral tissues, the sympathetic nervous system has been demonstrated to regulate key processes of immune cell function, such as the release of monocytes from the bone marrow compartment,[38] tissue programming of macrophages,[4] the cytokine expression profile of various immune cells,[39] and the antibody production of B cells.[40] A detailed picture of the signalling pathways and molecules involved that execute these diverse functions is only gradually evolving. Upon their activation, postganglionic sympathetic fibres release norepinephrine together with a number of cotransmitters (e.g. adenosine triphosphate). Norepinephrine exerts its function on recipient cells through the binding and activation of adrenoceptors, among which the beta-2-adrenoceptor and the beta-3-adrenoceptor have been assigned critical roles in regulating immune cell function or their mobilization.[37,41]

Given its central role in physiology, sympathetic control of immune cell functions has been studied in a number of immunological diseases and implicated in their pathogenesis. Rheumatoid arthritis, asthma, sepsis, colitis, and several other immunological diseases have all been linked to neuroinflammatory disorders, based on the abnormalities in ANS-dependent control of immune cell functions.[42] It is only recently that this important regulatory axis is investigated in the heart and in myocardial disease.[43] Gu *et al.*[44] observed a lower number of ED-1 cells (monocyte-derived macrophages) in ventricular myocardium upon treatment with artemisinin, which among other effects leads to a systemic inhibition of sympathetic nervous system function. Also, decreased reinnervation of remote myocardium post-MI has been reported upon depleting macrophages with systemic clodronate,[14] suggesting mutual control between immune cells and innervating sympathetic fibres. Although important, the above studies were not able to provide evidence that it is the activity of local, i.e., intracardiac nerves that control myocardial immune cells as opposed to systemic effects exerted by anti-sympathotonic or anti-macrophage agents. Our data obtained with local denervation now provide further evidence that sympathetic innervation controls local cardiac inflammation. The neural regulation of cardiac tissue macrophages appears to be involved in the development of cardiac failure, as interference with it was paralleled by altered development of disease. This model of local and surgical denervation and its applicability to genetically altered mice should prove useful to answer such questions and to delineate the underlying molecular mechanisms.

Our study also has a number of limitations, which should be addressed in future studies. This study was restricted to a single time point (i.e. 14 days) after MI and sympathectomy. It appears well conceivable that sympathetic denervation also affects the early phase of myocardial inflammation, where other immune cells (neutrophils and monocytes) are prevailing and several lines of evidence support this notion.[15,45] Nevertheless, we found the scar size after MI unaltered by SGx at the time of ischaemia, suggesting that sympathetic denervation protects the cardiac myocyte from post-MI dysfunction through mechanisms that are independent from the acute ischaemic loss of cardiac myocytes and possibly also independently from effects on early inflammation. It will be intriguing to test whether sympathetic denervation carried out at later time points (i.e. beyond the acute inflammatory phase) has similar effects on cardiac macrophage presence and overall cardiac function. Another aspect we did not address is whether sympathetic devervation interferes with vessel function and whether this would influence the inflammatory response after MI.

The answer to these questions may ultimately lead to more specific therapeutic interventions with myocardial inflammation. In the light of a generally modest long-term effect of systemically applied, broad anti-inflammatory treatments post-MI,[46,47] our data call for further studies into more specific and localized interventions.

Supplementary material

Supplementary material is available at *Cardiovascular Research* online.

References

1. Lymperopoulos A, Rengo G, Koch WJ. Adrenergic nervous system in heart failure. *Circ Res* 2013;**113**:739–753.

2. Dart AM, Du X-J, Kingwell BA. Gender, sex hormones and autonomic nervous control of the cardiovascular system. *Cardiovasc Res* 2002;**53**:678–687.

3. Sternberg EM. Neural regulation of innate immunity: a coordinated nonspecific host response to pathogens. *Nat Rev Immunol* 2006;**6**:318–328.

4. Gabanyi I, Muller PA, Feighery L, Oliveira TY, Costa-Pinto FA, Mucida D. Neuro-immune interactions drive tissue programming in intestinal macrophages. *Cell* 2016;**164**:378–391.

5. Scheiermann C, Kunisaki Y, Lucas D, Chow A, Jang J-E, Zhang D, Hashimoto D, Merad M, Frenette PS. Adrenergic nerves govern circadian leukocyte recruitment to tissues. *Immunity* 2012;**37**:290–301.

6. Cohn JN, Pfeffer MA, Rouleau J, Sharpe N, Swedberg K, Straub M, Wiltse C, Wright TJ. Adverse mortality effect of central sympathetic inhibition with sustained-release moxonidine in patients with heart failure (MOXCON). *Eur J Heart Fail* 2003;**5**:659–667.

7. Kaye D, Esler M. Sympathetic neuronal regulation of the heart in aging and heart failure. *Cardiovasc Res* 2005;**66**:256–264.

8. Oh Y-S, Jong AY, Kim DT, Li H, Wang C, Zemljic-Harpf A, Ross RS, Fishbein MC, Chen P-S, Chen LS. Spatial distribution of nerve sprouting after myocardial infarction in mice. *Heart Rhythm* 2006;**3**:728–736.

9. Cao J-M, Fishbein MC, Han JB, Lai WW, Lai A. C, Wu T-J, Czer L, Wolf PL, Denton T. A, Shintaku IP, Chen P-S, Chen LS. Relationship between regional cardiac hyperinnervation and ventricular arrhythmia. *Circulation* 2000;**101**:1960–1969.

10. Chen P. Sympathetic nerve sprouting, electrical remodeling and the mechanisms of sudden cardiac death. *Cardiovasc Res* 2001;**50**:409–416.

11. Nahrendorf M, Swirski FK. Monocyte and macrophage heterogeneity in the heart. *Circ Res* 2013;**112**:1624–1633.

12. Nahrendorf M, Pittet MJ, Swirski FK. Monocytes: protagonists of infarct inflammation and repair after myocardial infarction. *Circulation* 2010;**121**:2437–2445.

13. Swirski FK, Nahrendorf M. Leukocyte behavior in atherosclerosis, myocardial infarction, and heart failure. *Science* 2013;**339**:161–166.

14. Wernli G, Hasan W, Bhattacherjee A, Rooijen N, Smith PG. Macrophage depletion suppresses sympathetic hyperinnervation following myocardial infarction. *Basic Res Cardiol* 2009;**104**:681–693.

15. Sager HB, Dutta P, Dahlman JE, Hulsmans M, Courties G, Sun Y, Heidt T, Vinegoni C, Borodovsky A, Fitzgerald K, Wojtkiewicz GR, Iwamoto Y, Tricot B, Khan OF, Kauffman KJ, Xing Y, Shaw TE, Libby P, Langer R, Weissleder R, Swirski FK, Anderson DG, Nahrendorf M. RNAi targeting multiple cell adhesion molecules reduces immune cell recruitment and vascular inflammation after myocardial infarction. *Sci Transl Med* 2016;**8**:342ra80.

16. Pardini BJ, Lund DD, Schmid PG. Organization of the sympathetic postganglionic innervation of the rat heart. *J Auton Nerv Syst* 1989;**28**:193–201.

17. Franzoso M, Zaglia T, Mongillo M. Putting together the clues of the everlasting neuro-cardiac liaison. *Biochim Biophys Acta* 2016;**1863**:1904–1915.

18. Shen MJ, Zipes DP. Role of the autonomic nervous system in modulating cardiac arrhythmias. *Circ Res* 2014;**114**:1004–1021.

19. Florea VG, Cohn JN. The autonomic nervous system and heart failure. *Circ Res* 2014;**114**:1815–1826.

20. Manousiouthakis E, Mendez M, Garner MC, Exertier P, Makita T. Venous endothelin guides sympathetic innervation of the developing mouse heart. *Nat Commun* 2014;**5**:3918.

21. Choi J-H, Chang S-A, Choi J-O, Song YB, Hahn J-Y, Choi SH, Lee S-C, Lee S-H, Oh JK, Choe Y, Gwon H-C. Frequency of myocardial infarction and its relationship to angiographic collateral flow in territories supplied by chronically occluded coronary arteries. *Circulation* 2013;**127**:703–709.

22. Savastano LE, Castro AE, Fitt MR, Rath MF, Romeo HE, Muñoz EM. A standardized surgical technique for rat superior cervical ganglionectomy. *J Neurosci Methods* 2010;**192**:22–33.

23. Kalla Vyas A, Aerni-Flessner LB, Payne MA, Kovacs A, Jay PY, Hruz PW. Saxagliptin improves glucose tolerance but not survival in a murine model of dilated cardiomyopathy. *Cardiovasc Endocrinol* 2012;**1**:74–82.

24. Ram R, Mickelsen DM, Theodoropoulos C, Blaxall BC. New approaches in small animal echocardiography: imaging the sounds of silence. *Am J Physiol Heart Circ Physiol* 2011;**301**:H1765–H1780.

25. Nakajima H, Nakajima HO, Salcher O, Dittie AS, Dembowsky K, Jing S, Field LJ. Atrial but not ventricular fibrosis in mice expressing a mutant transforming growth factor-1 transgene in the heart. *Circ Res* 2000;**86**:571–579.

26. Ganesan J, Ramanujam D, Sassi Y, Ahles A, Jentzsch C, Werfel S, Leierseder S, Loyer X, Giacca M, Zentilin L, Thum T, Laggerbauer B, Engelhardt S. MiR-378 controls cardiac hypertrophy by combined repression of mitogen-activated protein kinase pathway factors. *Circulation* 2013;**127**:2097–2106.

27. Buitrago M, Lorenz K, Maass AH, Oberdorf-Maass S, Keller U, Schmitteckert EM, Ivashchenko Y, Lohse MJ, Engelhardt S. The transcriptional repressor Nab1 is a specific regulator of pathological cardiac hypertrophy. *Nat Med* 2005;**11**:837–844.

28. Nagatsu T, Nagatsu I. Tyrosine hydroxylase (TH), its cofactor tetrahydrobiopterin (BH4), other catecholamine-related enzymes, and their human genes in relation to the drug and gene therapies of Parkinson's disease (PD): historical overview and future prospects. *J Neural Transm* 2016;**123**:1255–1278.

29. Hartupee J, Mann DL. Neurohormonal activation in heart failure with reduced ejection fraction. *Nat Rev Cardiol* 2016;**14**:30–38.

30. Malpas SC. Sympathetic nervous system overactivity and its role in the development of cardiovascular disease. *Physiol Rev* 2010;**90**:513–557.

31. Bristow MR. Effect of baseline or changes in adrenergic activity on clinical outcomes in the -blocker evaluation of survival trial. *Circulation* 2004;**110**:1437–1442.

32. Jiang Y-H, Jiang P, Yang J-L, Ma D-F, Lin H-Q, Su W-G, Wang Z, Li X, Gonzalez GE. Cardiac dysregulation and myocardial injury in a 6-hydroxydopamine-induced rat model of sympathetic denervation. *PLoS One* 2015;**10**:1–19.

33. Singh JP, Kandala J, John Camm A. Non-pharmacological modulation of the autonomic tone to treat heart failure. *Eur Heart J* 2014;**35**:77–85.

34. Barber MJ, Mueller TM, Davies BG, Gill RM, Zipes DP. Interruption of sympathetic and vagal-mediated afferent responses by transmural myocardial infarction. *Circulation* 1985;**72**:623–631.

35. Miyauchi Y. Altered atrial electrical restitution and heterogeneous sympathetic hyperinnervation in hearts with chronic left ventricular myocardial infarction: implications for atrial fibrillation. *Circulation* 2003;**108**:360–366.

36. Zanoni FL, Simas R, Silva RG, da Breithaupt-Faloppa AC, Coutinho e Silva R. D S, Jatene FB, Moreira LFP. Bilateral sympathectomy improves postinfarction left ventricular remodeling and function. *J Thorac Cardiovasc Surg* 2017;**153**:855–863.e1.

37. Hanoun M, Maryanovich M, Arnal-Estapé A, Frenette PS. Neural regulation of hematopoiesis, inflammation, and cancer. *Neuron* 2015;**86**:360–373.

38. Méndez-Ferrer S, Lucas D, Battista M, Frenette PS. Haematopoietic stem cell release is regulated by circadian oscillations. *Nature* 2008;**452**:442–447.

39. Nance DM, Sanders VM. Autonomic innervation and regulation of the immune system (1987–2007). *Brain Behav Immun* 21:736–745.

40. Kasprowicz DJ, Kohm AP, Berton MT, Chruscinski AJ, Sharpe A, Sanders VM. Stimulation of the B cell receptor, CD86 (B7-2), and the 2-adrenergic receptor intrinsically modulates the level of IgG1 and IgE produced per B cell. *J Immunol* 2000;**165**:680–690.

41. Dutta P, Courties G, Wei Y, Leuschner F, Gorbatov R, Robbins CS, Iwamoto Y, Thompson B, Carlson AL, Heidt T, Majmudar MD, Lasitschka F, Etzrodt M, Waterman P, Waring MT, Chicoine AT, van der Laan AM, Niessen HWM, Piek JJ, Rubin BB, Butany J, Stone JR, Katus HA, Murphy SA, Morrow DA, Sabatine MS, Vinegoni C, Moskowitz MA, Pittet MJ, Libby P, Lin CP, Swirski FK, Weissleder R, Nahrendorf M. Myocardial infarction accelerates atherosclerosis. *Nature* 2012;**487**:325–329.

42. Pongratz G, Straub RH. The sympathetic nervous response in inflammation. *Arthritis Res Ther* 2014;**16**:1–12.

43. Abboud FM, Harwani SC, Chapleau MW. Autonomic neural regulation of the immune system: implications for hypertension and cardiovascular disease. *Hypertension* 2012;**59**:755–762.

44. Gu Y, Wang X, Wu G, Wang X, Cao H, Tang Y, Huang C. Artemisinin suppresses sympathetic hyperinnervation following myocardial infarction via anti-inflammatory effects. *J Mol Histol* 2012;**43**:737–743.

45. Wang Y, Liu J, Suo F, Hu H-S, Xue M, Cheng W-J, Xuan Y-L, Yan S-H. Metoprolol-mediated amelioration of sympathetic nerve sprouting after myocardial infarction. *Cardiology* 2013;**126**:50–58.

46. Saxena A, Russo I, Frangogiannis NG. Inflammation as a therapeutic target in myocardial infarction: learning from past failures to meet future challenges. *Transl Res* 2016;**167**:152–166.

47. Heymans S, Hirsch E, Anker SD, Aukrust P, Balligand J-L, Cohen-Tervaert JW, Drexler H, Filippatos G, Felix SB, Gullestad L, Hilfiker-Kleiner D, Janssens S, Latini R, Neubauer G, Paulus WJ, Pieske B, Ponikowski P, Schroen B, Schultheiss H-P, Tschöpe C, Bilsen M, van Zannad F, McMurray J, Shah AM. Inflammation as a therapeutic target in heart failure? A scientific statement from the Translational Research Committee of the Heart Failure Association of the European Society of Cardiology. *Eur J Heart Fail* 2009;**11**:119–129.